Three western pacific typhoons strengthened fire weather in the recent conflagration in northwest U.S.

Shih-Yu (Simon) Wang[1], Jacob Stuivenvolt Allen[1], Matthew LaPlante[2], and Jinho Yoon[3]

[1]Utah State University
[2]Utah State Univeristy
[3]Gwangju Institute of Science and Technology

November 21, 2022

Abstract

A heatwave and fire outbreak in the western United States in early September of 2020 resulted from an atmospheric wave train that spanned the Pacific Ocean basin. Days before the atmospheric waves developed in the U.S., three western Pacific tropical cyclones underwent an extratropical transition within an unprecedentedly short span of 12 days. Using a climate diagnostic approach and historical forecast data from the Global Ensemble Forecast System (GEFS), it was found that the amplitude of the atmospheric waves accompanying the western U.S. fire weather would have been reduced if not for the influence of these cyclones. Together, the recurving typhoons provided a significant source of Rossby wave activity toward North America-amplifying the ridge over the U.S. west coast while deepening the trough in central Canada. This anomalous circulation was a precursor to the severe frontal system that caused extreme winds in western Oregon-starting and rapidly spreading fire.

Three western pacific typhoons strengthened fire weather in the recent conflagration in northwest U.S.

S.-Y. Simon Wang[1], Jacob Stuivenvolt Allen[1], Matthew D. LaPlante[1,2], and Jin-Ho Yoon[3]

[1]Department of Plants, Soils and Climate, Utah State University, Logan, UT, USA

[2]Department of Journalism and Communication, Utah State University, Logan, UT, USA

[3]School of Earth Sciences and Environmental Engineering, Gwangju Institute of Science and Technology, Gwangju, South Korea

Corresponding author: Simon Wang (simon.wang@usu.edu)

Key Points:

- Anomalies of Rossby wave activity that began with recurving typhoons in the west Pacific heightened extreme weather events in North America.
- In observational and forecast data, these typhoons have exacerbated fire weather conditions through their impact to the jet-stream.
- Amplification of the trans-Pacific wave train led to a heatwave, strong winds and associated fires in western U.S.

Abstract

A heatwave and fire outbreak in the western United States in early September of 2020 resulted from an atmospheric wave train that spanned the Pacific Ocean basin. Days before the atmospheric waves developed in the U.S., three western Pacific tropical cyclones underwent an extratropical transition within an unprecedentedly short span of 12 days. Using a climate diagnostic approach and historical forecast data from the Global Ensemble Forecast System (GEFS), it was found that the amplitude of the atmospheric waves accompanying the western U.S. fire weather would have been reduced if not for the influence of these cyclones. Together, the recurving typhoons provided a significant source of Rossby wave activity toward North America—amplifying the ridge over the U.S. west coast while deepening the trough in central Canada. This anomalous circulation was a precursor to the severe frontal system that caused extreme winds in western Oregon—starting and rapidly spreading fire.

Plain Language Summary

The weather pattern accompanying the heatwave in California and rapidly spreading fires in Oregon in early September 2020 can be traced back to an unexpected source: typhoons in the western Pacific. Three typhoons ran into the Korean Peninsula within two weeks leading up to the heatwave and fire events. Together, Typhoon Bavi, Typhoon Maysak and Typhoon Haishe contained substantial energy to perturb the jet-stream—creating a rippling atmospheric wave train that had a pronounced effect on the hot-dry weather of western U.S. This study uses forecast models and weather observations to show that these typhoons amplified areas of high pressure and low pressure in North America leading to the intense winds which rapidly spread fire in Oregon and Washington. While the impacts of climate change on these events were not evaluated in this study, the implication is that the effect of weather extremes is not always limited to the region in which those extremes occur.

1 Introduction

The unprecedented Oregon wildfires that have intensified rapidly on September 7, 2020, have burned over 1 million acres and killed 23 people (as of 09/20/20), with about 500,000 people evacuated. The remarkable spread of fires occurred in association with an extreme wind event that brought 25 to 50 mph winds to western Oregon (https://wildfiretoday.com/). This wind event, which lasted through September 8, 2020, (Figure 1a) was caused by a powerful frontal system that formed an unseasonably strong east-west pressure gradient, accompanied by an amplified atmospheric ridge to its west. This amplified ridge was also blamed for a California heatwave in the days before the fires (https://www.npr.org/). Together, the heat-trapping western ridge and the front-producing eastern trough formed a quasi-stationary wave over North America, one that had its origins in the western North Pacific (the evolution of this circulation can be viewed at http://tinyurl.com/TyphoonsToHeatWave). Days before, the western North Pacific saw three strong tropical cyclones that passed through the Korean Peninsula in rapid succession: Typhoon Bavi (which reached Korea on August 26), Typhoon Maysak (which reached Korea on September 2), and Typhoon Haishen (which reached Korea and Japan on September 6). All three typhoons had maximum sustained wind speeds greater than 118 km/h (74 mph) and all of them recurved and went through an extratropical transition. It was the first time on record that Korea had been hit by three consecutive typhoons within two weeks, and each typhoon was responsible for releasing Rossby wave energy into the midlatitude jet stream.

The meteorological community has known that as a typhoon recurves and undergoes extratropical transition [*Jones et al.*, 2003], its interaction with the jet stream can perturb the extratropical flow and trigger high-impact weather events far downstream (e.g., [*Agustí-Panareda et al.*, 2005; *Harr and Dea*, 2009; *Hodyss and Hendricks*, 2010; *Namias*, 1963; *Pantillon et al.*, 2013]). As shown in Figure 2a, *Archambault et al.* [2013] portrayed how a recurving typhoon in the western North Pacific can amplify a high-latitude ridge over western North America and an early season cold-air outbreak over the central United States. Generally a recurving typhoon is steered ahead of a trough and contributes to wave amplification to the east and jet stream intensification to the north. Extratropical cyclogenesis is then enhanced in conjunction with Rossby wave dispersion, which amplifies a downstream ridge over western North America. The amplified ridge provides dynamic forcing for a cold-air outbreak east of the Rocky Mountains along with a baroclinic/low-pressure trough [*Archambault et al.*, 2013]. This situation bears striking resemblance to what has transpired during early September 2020, but the extent to which *three* recurving typhoons interacting with the extratropical flows in East Asia contributed to the remarkable North American circulation anomaly is unclear. This study aims to examine the role of the three consecutive typhoons, an unprecedented event of its own, in the record heat and wind events in the West Coast.

2 Data

To evaluate the impact of western Pacific tropical cyclones (typhoons) on the recent western U.S. heatwave and fire outbreak, this study used archived forecast data from the National Centers for Environmental Prediction (NCEP) Global Ensemble Forecast System (GEFS). The GEFS is produced four times daily with forecast times out to 16 days after the initialization time. Twenty-one ensemble members at 1° resolution are run in each initialization, with perturbations in the initial conditions gathered from the operational hybrid Global Data

Assimilation System 80-member Ensemble Kalman Filter [*Whitaker et al.*, 2008]. GEFS's initializations with observed tropical storms use a tropical storm relocation technique to adjust the model's central storm location to more accurately represent observations and offer more accurate possibilities for tropical cyclone evolution due to initial conditions perturbations [*Zhou et al.*, 2016]. We adopted the historical forecast data that were initialized from 00z August 23 (as far back as the dataset goes) through 18z August 30, 2020 (to provide enough spread for different scenarios). For any given day in September (e.g., 12Z 9/1), the forecast data consist of 4 x 8 x 21 = 672 members for the analysis. For observational data analysis, we used the 6-h NCEP-NCAR Reanalysis with a 2.5˚ spatial resolution from 1948 to 2020 [*Kalnay et al.*, 1996].

3 Results and Discussions

3.1 Putting the wind event into perspective

By averaging the 2-meter zonal wind field over western Oregon (domain outlined in Figure 1b inset, 125˚-121˚W, 42˚-48˚N), we plotted the daily time series of zonal wind for each year including 2020 (black line; negative value indicates easterly wind). Compared with the 1948-2019 period, the maximum easterly occurring on 8 September 2020 wind is indeed a record event. Strong easterly wind causes downslope adiabatic warming/drying that enhances fire weather conditions. The fact that the 2020 record easterly wind occurred during the climatologically westerly wind regime and at the height of Oregon's fire season is what made the wildfires spread so rapidly. Comparison between data periods before and after 1979 also suggests that the fluctuation in the day-to-day surface winds over western Oregon has increased slightly. Note that actual (station) wind speeds in Oregon are greater than what the reanalysis data can describe, but the data during all the 1948-2020 period in Figure 1b are consistent and so, it can provide a historical perspective.

3.2 Diagnostic analysis

To analyze the stationary wave pattern evolution over the North Pacific and North America, we computed the Rossby wave activity flux (WAF) using the derivation of *Takaya and Nakamura* [2001] to depict propagating planetary waves and associated wave energy in association with the mean background flow. WAF is linear and independent of time periods, so we averaged the 100-300 hPa geopotential height and WAF and plotted their multi-day means, from August 25-28 through September 8-12 (Figure 2b). The three typhoons are indicated in the corresponding time period in which they propagated northward past 35˚N while approaching Korea. Snapshots of these typhoons are plotted in Figure 2c in terms of 200-hPa geopotential height and 925-hPa wind vectors using GEFS initial data and, in each one, the amplified high-pressure ridge to the east is patent. The Oregon extreme wind event on August 8 is shown in the bottom of Figure 2c for comparison.

From late August through early September, the striking feature of wave amplification in the geopotential height is revealed from the eastward propagating WAF across the North Pacific. It takes 3-4 days for a recurving typhoon in the midlatitude to generate an amplified ridge over western North America [*Grams and Archambault*, 2016], and Figure 2b indeed describes such a feature in terms of the WAF propagation: Typhoon Bavi generated an area of significant WAF to its immediate east that amplified the ridge around 150˚E (8/25-28 in Figure 2b). Four days later, increased WAF appeared in the Aleutian low and amplified the downstream ridge near western North America (8/28-9/1). This enhanced ridge then generated its own WAF in central Canada, deepening the trough there (8/31-9/4). Meanwhile, Typhoon Maysak generated new fluxes of WAF that enhanced the ridge over Japan, and this further amplified the Aleutian low and the downstream ridge near California. During 9/4-9/8, Typhoon Haishen repeated the process by strengthening the source and propagation of WAF over the course of 5 days, making the West Coast ridge and central Canada trough even stronger. We now know that this enhanced ridge contributed to the California heatwave that reached its severity on September 6, followed by the collapse of cold air that plowed through the intermountain West in the next two days. During 9/8-9/12 and after the frontal outbreak, the western North Pacific ridge weakened and so did the North American wave pattern. This episode of cross-Pacific wave train was most pronounced during 9/4-9/8, associated with the heatwave in California and extreme wind events in Oregon, as well as record winds in Utah, where thousands of trees were uprooted, homes were destroyed and at least one death (https://www.sltrib.com/).

3.3 Forecast data investigation

Diagnostic analysis using the WAF calculation is useful, however, it only depicts the possible source and magnitude of Rossby wave dispersion. It does not identify whether the North American weather that predated the historic fires would have happened without the western Pacific typhoons. Moreover, atmospheric internal variability can also amplify the trans-Pacific wave train without requiring external forcing like a recurving typhoon [*Orlanski and Sheldon*, 1995; *Schroeder et al.*, 2016]. To account for these unknowns, we used the GEFS 16-day forecast initialized before September to provide the closest possible scenarios of the atmospheric circulation with and without the forecast typhoons.

For example, to investigate the effect of Typhoon Maysak's extratropical transition (e.g., 00Z September 2) on the Oregon wind event (00Z September 8), we used the center value of 1000-hPa geopotential height (HGT_{1000}) at the typhoon's observed location to determine whether the forecast captured the typhoon. Using HGT_{1000} is useful because all typhoons have a negative value at their center and so, any forecast time step that shows positive value would be considered a missed forecast. Typhoon Maysak on 00Z September 2, for instance, consists of various forecast steps as long as 264 hours (initialized on 00Z 8/23) and as short as 78 hours (initialized on 18Z 8/30). However, each typhoon also requires a different threshold of HGT_{1000} because of its proximity to the forecast initial time. Our principle is to maintain balanced member sizes for the "with typhoon" and "without typhoon" groups, with at least 30 members in either group. It is expected that the closer the initialization is to the typhoon's presence, the more accurate GEFS captures it, so the member size in the "without typhoon" group likely results from the longer forecast steps (earlier forecasts). Since forecast skill is not the focus here, we did not discriminate how far back or how different the initial time steps are in the composite analysis.

For Typhoon Bavi (6Z August 26), data up to 00Z August 26 was used to produce the forecast groups based on two thresholds: 1 and 2 standard deviations of all forecasts *above* the observed value of center HGT_{1000}. Forecast values less than 1 standard deviation of the ensemble HGT_{1000} were considered "with typhoon" and those greater than 2 standard deviation were grouped into "without typhoon". Figure 3a (inset left) shows the two groups of Typhoon Bavi from the forecast and, while both groups depict a low-pressure system, the "without typhoon" group (top) indicates a much weaker central pressure than the "with typhoon" group (bottom). Figure 3a shows the composite 250-hPa geopotential height (HGT_{250}) on September 1 of the two groups. The "with typhoon" HGT_{250} (golden contours) depicts a stronger ridge in western North America accompanied by a slightly deeper trough in the upper Midwest, than the "without typhoon" HGT_{250} (blue contours). We repeated the similar composite analysis using all August 23-30 forecast data for Typhoon Maysak based on its September 2 condition. Since Typhoon Maysak was at least 54 hours away from the nearest initial forecast, we found members that totally missed the typhoon. Therefore, the composite HGT_{1000} (Figure 3b inset) shows a marked difference with and without the typhoon. The impact of Typhoon Maysak on September 8's HGT_{250} pattern (Figure 3b) includes an amplification of the trans-Pacific wave train all the way through eastern North America, which accompanies a distinctly stronger ridge over California (which is closer to observation).

The observed circulation pattern on September 8 was marked by a considerably more undulating appearance than that with Typhoon Maysak (Figure 3b; purple dotted contours vs. golden contours), likely because there was another extratropical transition by Typhoon Haishen that took place a couple of days before. Figure 3c shows the HGT_{1000} composites of Typhoon Haishen (00Z September 6) and associated HGT_{250} patterns on September 8. Due to the long-range forecast steps of Typhoon Haishen, even the "with typhoon" composite of HGT_{1000} appears weak. Nonetheless, the difference of the resultant trans-Pacific wave train between the two groups is remarkable. The "with typhoon" HGT_{250} composite clearly depicts the amplified wave train and phase that are in good agreement with the observed, even though by September 8 the forecast had approached their limit (10-16 days out). The amplified ridge-trough pattern over North American was well captured, despite missing the "Z" shape over the Rocky Mountains associated with the powerful frontal system. We also note that more than 60% of the members that captured Typhoon Haishen also forecasted Typhoon Maysak, so the realistic wave train as depicted by the "with typhoon" HGT_{250} also signifies the combined Rossby wave dispersion effects from these almost back-to-back typhoons.

Though not shown here, we found that Typhoon Bavi alone (August 26) did not produce a substantial lingering effect on the North American wave pattern after September 4. However, Typhoon Bavi did contribute to the early September ridge over western North America (Figure 3a) leading to the buildup of hot and dry condition in West Coast, which worsened the drought conditions in Oregon (https://droughtmonitor.unl.edu/). For verification purposes, we conducted a reversed approach by using the North American wave pattern as the basis of evaluation, in order to assess the difference in the forecast typhoons (see Supplemental Text). The results are consistent that, for the North American wave pattern that was missed by the forecast, the prior typhoon tends to be missed or underpredicted (Supplemental Figures S1-3). Conversely, when the North American wave pattern was realistically depicted, the preceding typhoons were much better forecasted.

3.4 Perspective in a changing climate

The analysis presented here does not have the means to address the role of climate change, though it is prudent to consider climate change in the severity of these September 2020 extreme events. The extreme wind event in western Oregon was unprecedented but did not appear to be associated with a noticeable trend. However, peripheral evidence from literature may offer some clues. First, the long-term increase in aridity over western North America has been reported since late 20th century [*Cook et al.*, 2004] and this trend has continued in recent droughts over California and the western region [*Diffenbaugh et al.*, 2015; *Williams et al.*, 2015]. Warming and increased aridity contribute to higher risk of severe wildfires [*Bryant and Westerling*, 2014; *Dennison et al.*, 2014; *Westerling et al.*, 2006]. Second, the observed increase in the tropical ocean-atmosphere interactions that result in amplified teleconnection patterns also contributed to the buildup of fuel and potential burn areas in California [*Swain et al.*, 2018; *Yoon et al.*, 2015] and the western U.S. [*Holden et al.*, 2018; *Voelker et al.*, 2019]. The marked amplification of the atmospheric waves over North Pacific and North America during early September 2020 is in agreement with the documented change in the summertime short-wave pattern along the jet stream [*Kornhuber et al.*, 2019; *Mann et al.*, 2017; *Wang et al.*, 2013]. Lastly, the long-term change in East Asian summer monsoon (EASM) may be relevant, given the recent trend towards an enhanced EASM lifecycle consisting of the onset, break, and revival phases [*Wang et al.*, 2019]. The revival phase of EASM is largely attributed to typhoon rainfall and the observed poleward shift of western North Pacific tropical cyclones associated with the warmer ocean [*Sharmila and Walsh*, 2018; *Sun et al.*, 2019] echoes the three consecutive typhoons recurving and hitting Korea this year. Given the typhoon impacts on western North America during a time of the year that coincides with the peak fire season, it is crucial that we develop a better understanding of the extent to which the warming climate may increase the extratropical transition of fall typhoons in the west Pacific.

Summer 2020 also saw a La Niña event developed during hurricane seasons in the Northern Hemisphere (https://www.noaa.gov/). A developing La Niña is known to worsen the southwest U.S. drought (http://nytimes.com) and it also modulates the western North Pacific tropical cyclone activity by causing them to form in higher latitudes and recurve more easily [*Chen et al.*, 2006; *Han et al.*, 2016]. Interannual variation like the ongoing La Niña cannot be overlooked in future diagnostic analysis of this remarkable series of extreme events in early September 2020.

4 Conclusions

Intrinsic meteorological variations and remote influences of atmospheric circulation are demonstrated in the case of extreme events in the western U.S. in September 2020. The rapid amplification of the atmospheric waves over western North America, leading to extreme heat and dangerous fire weather, can be attributed to traceable effects from significant weather systems far away. The succession of three recurving typhoons, which passed through the Korea Peninsula within two weeks of one another, appears to have generated strong and persistent Rossby wave activity to enhance the upper-tropospheric circulation—amplifying the ridge in western North America and the trough in central Canada. The use of GEFS 16-day forecast and reanalysis data offers an example for synoptic attribution of extreme weather events that can be done near real-time. Through it, we determined the difference between possible atmospheric scenarios for realistic typhoon forecasts (which went through an extratropical transition and released energy into the jet stream), and “missed,” or more unrealistic, typhoon forecasts. The results portray a consistent picture of Rossby wave energy being channeled through the trans-Pacific wave train toward North America. If the warming ocean conditions do migrate fall typhoons poleward, as suggested in the literature, then the chances of such remote influence on western North America may increase. This aspect deserves further analysis.

Acknowledgments

All GEFS and reanalysis data sets are publicly available at https://nomads.ncep.noaa.gov/txt_descriptions/GFS_doc.shtml and the authors thank the U.S. government for providing these important weather data free of charges. Research fundings from the U.S. Department of Energy/Office of Science under Award Number DE-SC0016605 and the SERDP project RC20-3056 are acknowledged.

Reference:

Agustí-Panareda, A., S. L. Gray, G. C. Craig, and C. Thorncroft (2005), The extratropical transition of Tropical Cyclone Lili (1996) and its crucial contribution to a moderate extratropical development, Monthly weather review, 133(6), 1562-1573.

Archambault, H. M., L. F. Bosart, D. Keyser, and J. M. Cordeira (2013), A climatological analysis of the extratropical flow response to recurving western North Pacific tropical cyclones, Monthly weather review, 141(7), 2325-2346.

Bryant, B. P., and A. L. Westerling (2014), Scenarios for future wildfire risk in California: links between changing demography, land use, climate, and wildfire, Environmetrics, n/a-n/a, doi: 10.1002/env.2280.

Chen, T.-C., S.-Y. Wang, and M.-C. Yen (2006), Interannual Variation of the Tropical Cyclone Activity over the Western North Pacific, Journal of Climate, 19(21), 5709-5720, doi: doi:10.1175/JCLI3934.1.

Cook, E. R., C. A. Woodhouse, C. M. Eakin, D. M. Meko, and D. W. Stahle (2004), Long-term aridity changes in the western United States, Science, 306(5698), 1015-1018.

Dennison, P. E., S. C. Brewer, J. D. Arnold, and M. A. Moritz (2014), Large wildfire trends in the western United States, 1984–2011, Geophysical Research Letters, 41(8), 2928-2933.

Diffenbaugh, N. S., D. L. Swain, and D. Touma (2015), Anthropogenic warming has increased drought risk in California, Proceedings of the National Academy of Sciences, 112(13), 3931-3936.

Grams, C. M., and H. M. Archambault (2016), The key role of diabatic outflow in amplifying the midlatitude flow: A representative case study of weather systems surrounding western North Pacific extratropical transition, Monthly Weather Review, 144(10), 3847-3869.

Han, R., H. Wang, Z.-Z. Hu, A. Kumar, W. Li, L. N. Long, J.-K. E. Schemm, P. Peng, W. Wang, and D. Si (2016), An assessment of multimodel simulations for the variability of western North Pacific tropical cyclones and its association with ENSO, Journal of Climate, 29(18), 6401-6423.

Harr, P. A., and J. M. Dea (2009), Downstream development associated with the extratropical transition of tropical cyclones over the western North Pacific, Monthly weather review, 137(4), 1295-1319.

Hodyss, D., and E. Hendricks (2010), The resonant excitation of baroclinic waves by the divergent circulation of recurving tropical cyclones, Journal of the atmospheric sciences, 67(11), 3600-3616.

Holden, Z. A., A. Swanson, C. H. Luce, W. M. Jolly, M. Maneta, J. W. Oyler, D. A. Warren, R. Parsons, and D. Affleck (2018), Decreasing fire season precipitation increased recent western US forest wildfire activity, Proceedings of the National Academy of Sciences, 115(36), E8349-E8357.

Jones, S. C., P. A. Harr, J. Abraham, L. F. Bosart, P. J. Bowyer, J. L. Evans, D. E. Hanley, B. N. Hanstrum, R. E. Hart, and F. Lalaurette (2003), The extratropical transition of tropical cyclones: Forecast challenges, current understanding, and future directions, Weather and Forecasting, 18(6), 1052-1092.

Kalnay, E., et al. (1996), The NCEP/NCAR 40-Year Reanalysis Project, Bulletin of the American Meteorological Society, 77(3), 437-471, doi: doi:10.1175/1520-0477(1996)077<0437:TNYRP>2.0.CO;2.

Kornhuber, K., S. Osprey, D. Coumou, S. Petri, V. Petoukhov, S. Rahmstorf, and L. Gray (2019), Extreme weather events in early summer 2018 connected by a recurrent hemispheric wave-7 pattern, Environmental Research Letters, 14(5), 054002.

Mann, M. E., S. Rahmstorf, K. Kornhuber, B. A. Steinman, S. K. Miller, and D. Coumou (2017), Influence of Anthropogenic Climate Change on Planetary Wave Resonance and Extreme Weather Events, 7, 45242, doi: 10.1038/srep45242 https://www.nature.com/articles/srep45242#supplementary-information.

Namias, J. (1963), Large-scale air-sea interactions over the North Pacific from summer 1962 through the subsequent winter, Journal of Geophysical Research, 68(22), 6171-6186.

Orlanski, I., and J. P. Sheldon (1995), Stages in the energetics of baroclinic systems, Tellus A, 47(5), 605-628.

Pantillon, F., J. P. Chaboureau, C. Lac, and P. Mascart (2013), On the role of a Rossby wave train during the extratropical transition of Hurricane Helene (2006), Quarterly Journal of the Royal Meteorological Society, 139(671), 370-386.

Schroeder, M., S.-Y. S. Wang, R. R. Gillies, and H.-H. Hsu (2016), Extracting the tropospheric short-wave influences on subseasonal prediction of precipitation in the United States using CFSv2, Climate Dynamics, 1-8, doi: 10.1007/s00382-016-3314-1.

Sharmila, S., and K. Walsh (2018), Recent poleward shift of tropical cyclone formation linked to Hadley cell expansion, Nature Climate Change, 8(8), 730-736.

Sun, J., D. Wang, X. Hu, Z. Ling, and L. Wang (2019), Ongoing poleward migration of tropical cyclone occurrence over the western North Pacific Ocean, Geophysical Research Letters, 46(15), 9110-9117.

Swain, D. L., B. Langenbrunner, J. D. Neelin, and A. Hall (2018), Increasing precipitation volatility in twenty-first-century California, Nature Climate Change, 8(5), 427-433.

Takaya, K., and H. Nakamura (2001), A Formulation of a Phase-Independent Wave-Activity Flux for Stationary and Migratory Quasigeostrophic Eddies on a Zonally Varying Basic Flow, Journal of the Atmospheric Sciences, 58(6), 608-627, doi: doi:10.1175/1520-0469(2001)058<0608:AFOAPI>2.0.CO;2.

Voelker, S. L., A. G. Merschel, F. C. Meinzer, D. E. Ulrich, T. A. Spies, and C. J. Still (2019), Fire deficits have increased drought sensitivity in dry conifer forests: Fire frequency and tree-ring carbon isotope evidence from Central Oregon, Global change biology, 25(4), 1247-1262.

Wang, S.-Y., R. E. Davies, and R. R. Gillies (2013), Identification of extreme precipitation threat across midlatitude regions based on short-wave circulations, Journal of Geophysical Research: Atmospheres, 118(19), 2013JD020153, doi: 10.1002/jgrd.50841.

Wang, S.-Y., H. Kim, D. Coumou, J.-H. Yoon, L. Zhao, and R. R. Gillies (2019), Consecutive extreme flooding and heat wave in Japan: Are they becoming a norm?, Atmospheric Science Letters, 20(10), e933, doi: 10.1002/asl.933.

Westerling, A. L., H. G. Hidalgo, D. R. Cayan, and T. W. Swetnam (2006), Warming and Earlier Spring Increase Western U.S. Forest Wildfire Activity, Science, 313(5789), 940-943, doi: 10.1126/science.1128834.

Whitaker, J. S., T. M. Hamill, X. Wei, Y. Song, and Z. Toth (2008), Ensemble Data Assimilation with the NCEP Global Forecast System, Monthly Weather Review, 136(2), 463-482, doi: 10.1175/2007mwr2018.1.

Williams, A. P., R. Seager, J. T. Abatzoglou, B. I. Cook, J. E. Smerdon, and E. R. Cook (2015), Contribution of anthropogenic warming to California drought during 2012–2014, Geophysical Research Letters, 42(16), 6819-6828.

Yoon, J.-H., S.-Y. S. WANG, R. R. GILLIES, L. HIPPS, B. KRAVITZ, and P. J. RASCH (2015), 2. Extreme Fire Season in California: A Glimpse Into The Future?, Bull Am Meteorol Soc, 96, S5-9.

Zhou, X., Y. Zhu, D. Hou, and D. Kleist (2016), A Comparison of Perturbations from an Ensemble Transform and an Ensemble Kalman Filter for the NCEP Global Ensemble Forecast System, Weather and Forecasting, 31(6), 2057-2074, doi: 10.1175/waf-d-16-0109.1.

Figures 1-3.

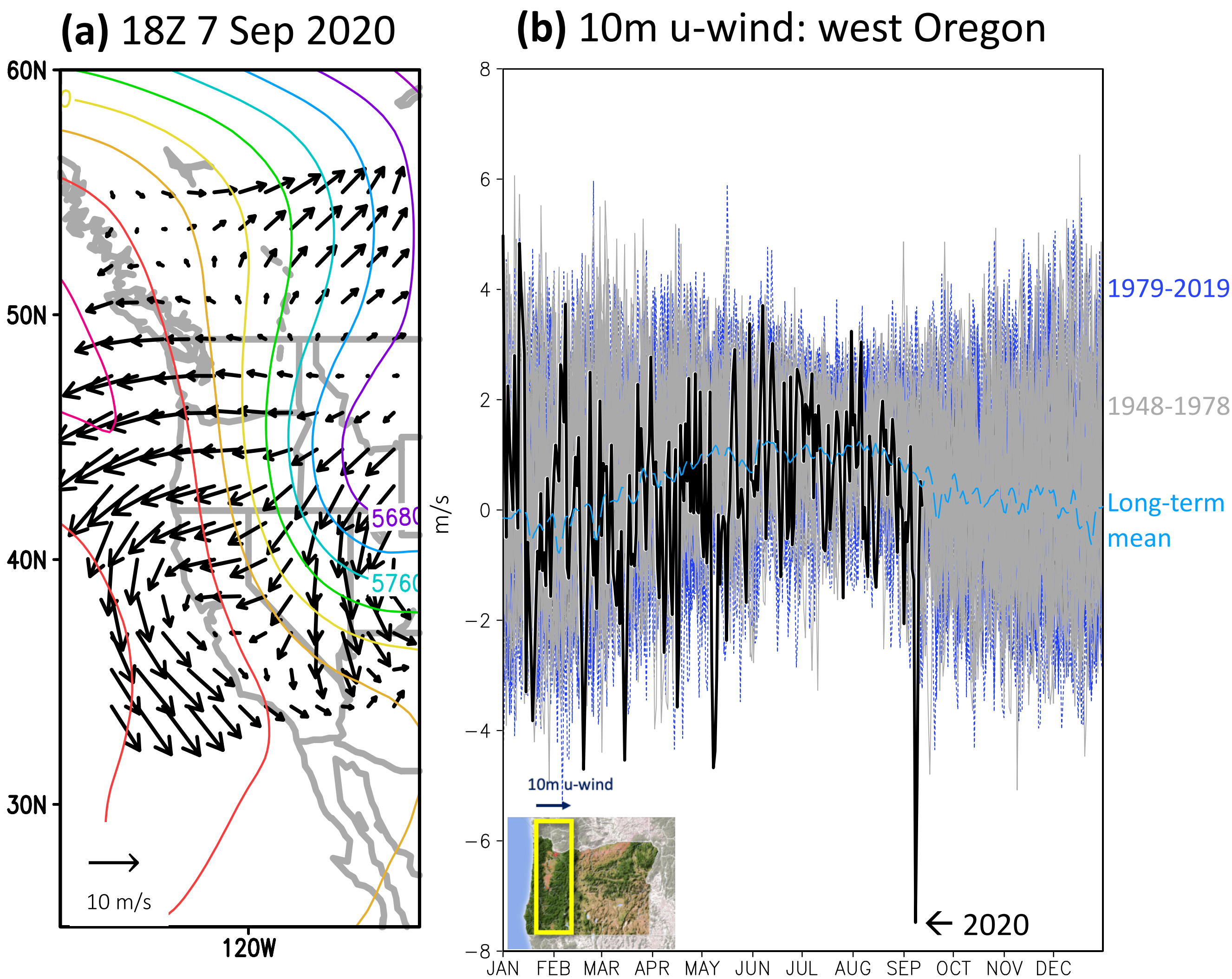

Figure 1

(a) The onset of widespread Oregon wildfires on 7 September 2020 in terms of 500-hPa geopotential height contours and 2-meter wind vectors, showing the extreme wind event at 18Z. (b) Daily time series of 10-meter zonal wind averaged over western Oregon (box area in lower-left map) in 2020 as thick black line and during 1948-1978 as gray lines and 1979-2019 as blue lines. Notice the extreme negative value indicating the record easterly wind event on 8 September 2020. The climatological zonal wind evolution is added as the light blue line.

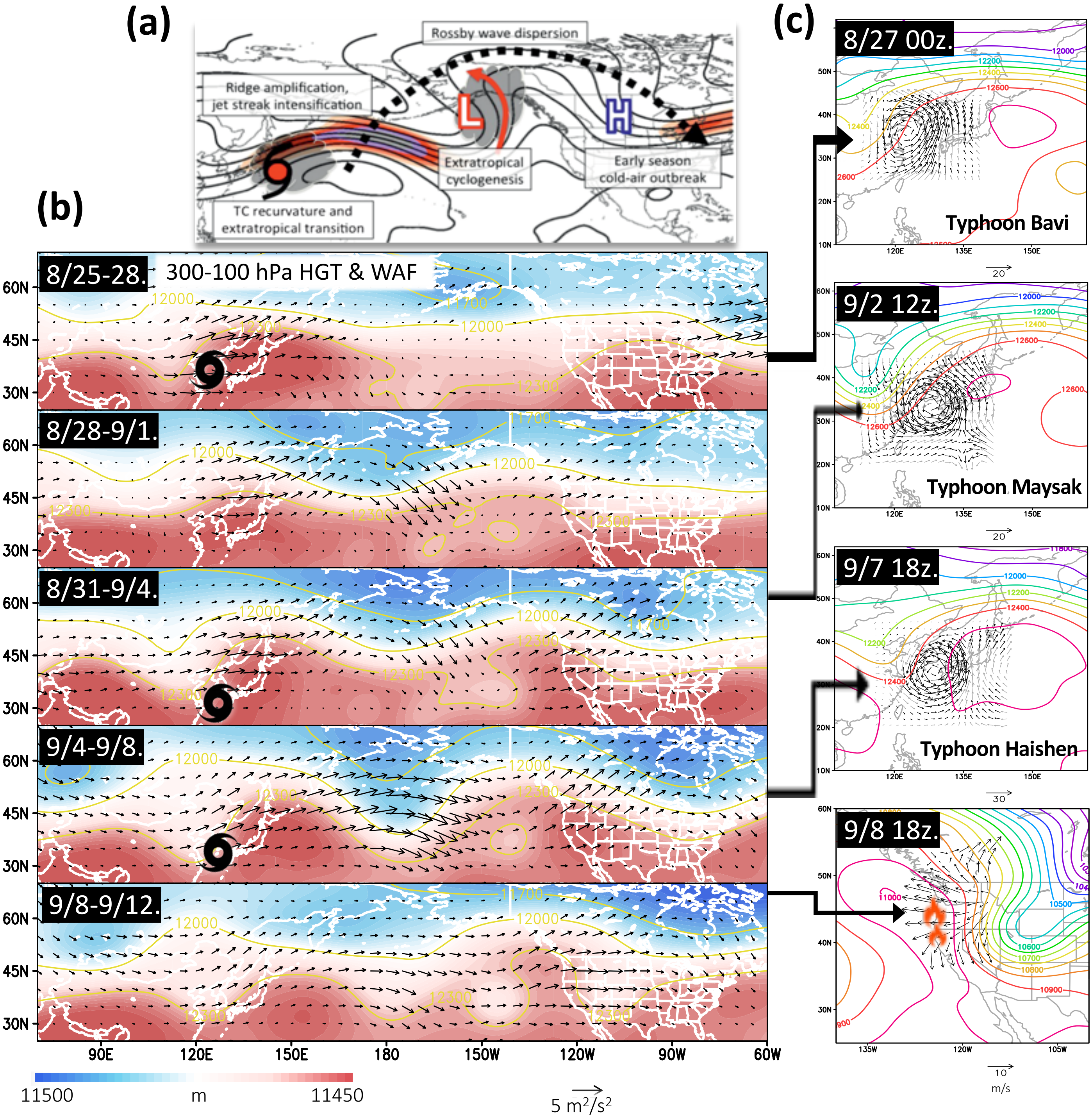

Figure 2

(a) Schematic diagram adopted from *Archambault et al.* [2013] depicting the process in which a recurving typhoon near Japan goes through extratropical transition and generates Rossby wave dispersion downstream, enhancing the ridge pattern in western North America. **(b)** Composites of 100-300-hPa averaged geopotential height (shadings and golden contours) and wave activity flux (vectors) over 4-5 days as indicated by the date range in upper left. Typhoon symbols indicate the extratropical transition points of the three typhoons near 130˚E. **(c)** Regional depiction of each typhoons (top 3) at the time indicated in upper-left corner and typhoon name in lower right, in terms of the 250-hPa geopotential height contours and 925-hPa winds, as well as the peak wind event in West Coast (bottom, with fire symbols in western Oregon); note the different wind scales.

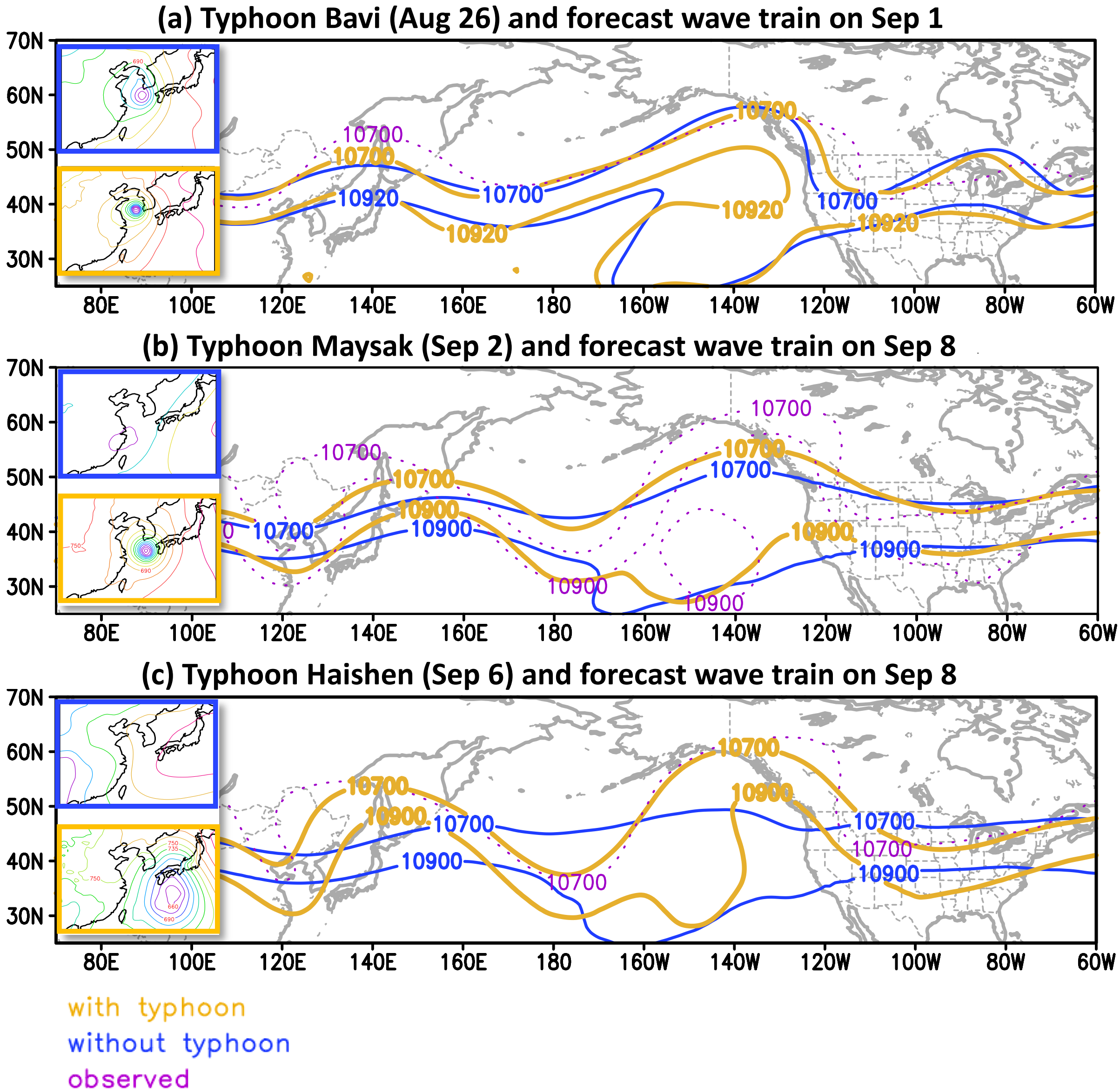

Figure 3

Composite groups of 925-hPa geopotential height for "without typhoon" (top, blue outline) and "with typhoon" (bottom, golden outline) of each forecast typhoon and the composite 250-hPa geopotential height contours in the corresponding colors, overlaid with the reanalysis height as dotted purple contour, for **(a)** Typhoon Bavi of August 26 and the wave train on September 1, **(b)** Typhoon Maysak of September 2 and the September 8 wave train, and **(c)** Typhoon Haishen of September 6 and the September 8 wave train. Note the difference in the ridge patterns over western North America and the trough patterns in the central U.S.

Geophysical Research Letters

Supporting Information for

Three western pacific typhoons strengthened fire weather in the recent conflagration in northwest U.S.

S.-Y. Simon Wang[1], Jacob Stuivenvolt Allen[1], Matthew LaPlante[1,2], and Jin-Ho Yoon[3]

[1]Department of Plants, Soils and Climate, Utah State University, Logan, UT, USA

[2]Department of Journalism and Communication, Utah State University, Logan, UT, USA

[3]School of Earth Sciences and Environmental Engineering, Gwangju Institute of Science and Technology, Gwangju, South Korea

Contents of this file

Text S1.

By following the forecast evaluation based on typhoons as shown in Figure 3, we adopted a reverse approach by evaluating the North American circulation pattern and used the hit-and-miss forecast grouping to examine the preceding typhoon. Here, we applied the spatial correlation analysis to the 250-hPa geopotential height eddy ($HGT_{250}E$, with the zonal mean removed) between forecast and reanalysis within the domain outlined in Figure S1; we also computed the variance of $HGT_{250}E$ over this domain. Then, we used correlation coefficients less than 0.3 and the variance ratio smaller than 40% (of the observed) as the threshold to identify forecast that is a “miss” of the North American circulation pattern and associated typhoon. By using correlation coefficients greater than 0.8 and variance smaller than 60% as the threshold, we identified the forecast as a “hit”. The resultant composite circulations are shown in Figures S1-S3.

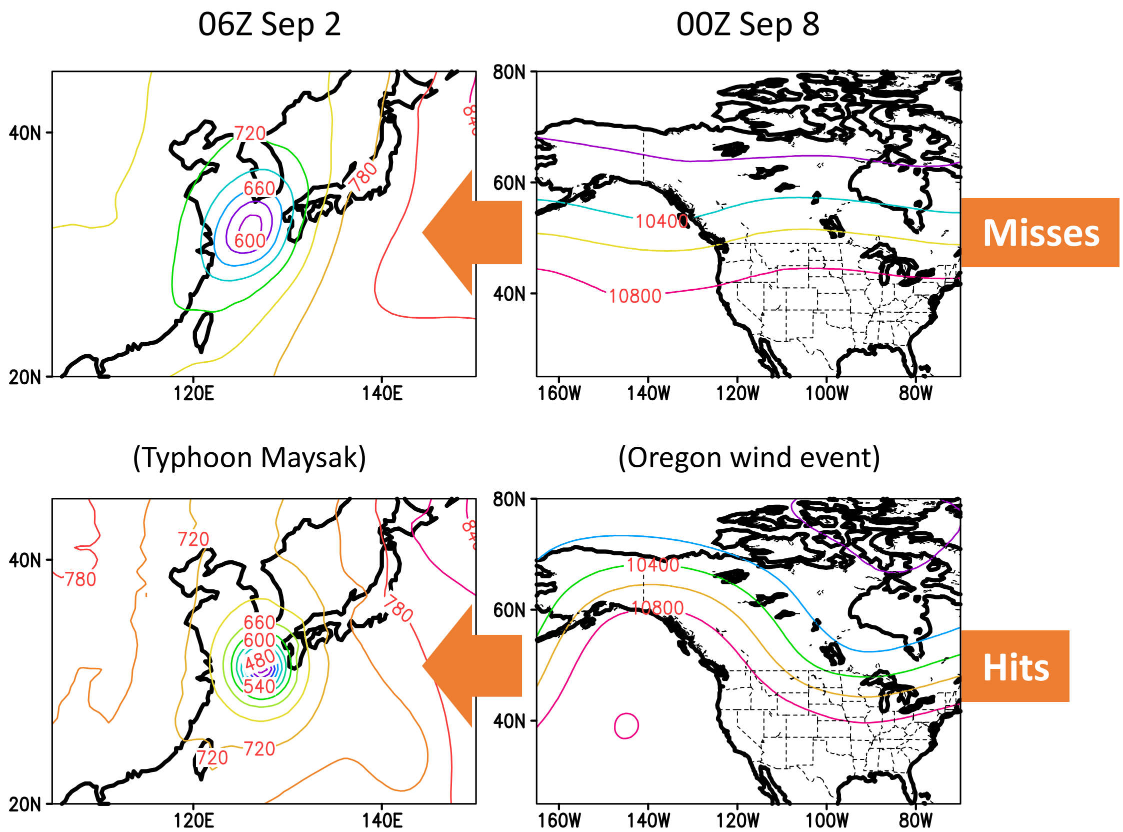

Figure S1. The “missed” September 8 North American wave pattern at 250 hPa and associated typhoon on September 2 (Maysak) at 925 hPa in terms of geopotential height (unit: meter). The orange arrows indicate the direction of our evaluation that is based on the North American circulation. Note the high-amplitude ridge and trough in western and central North America, respectively.

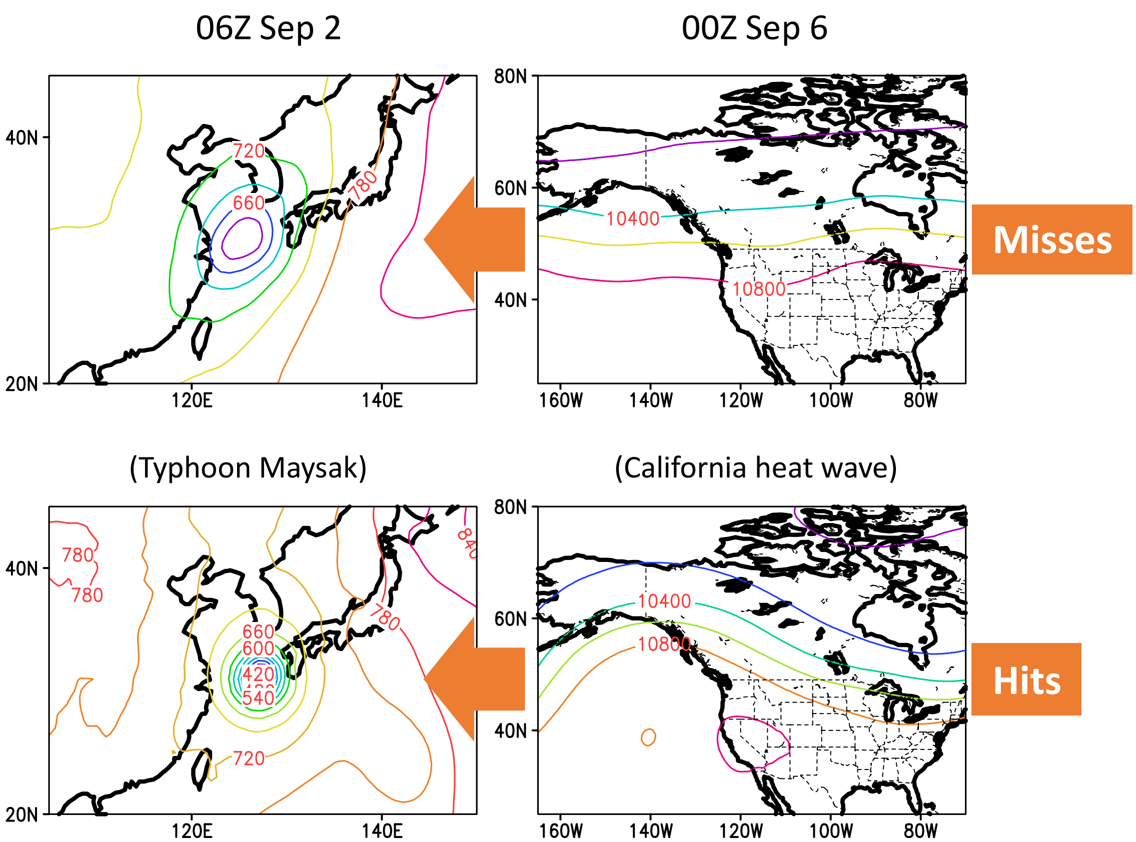

Figure S2. Same as Figure S1 but for the September 6 North American circulation pattern, in which the California heatwave occurred, and associated forecast difference of Typhoon Maysak.

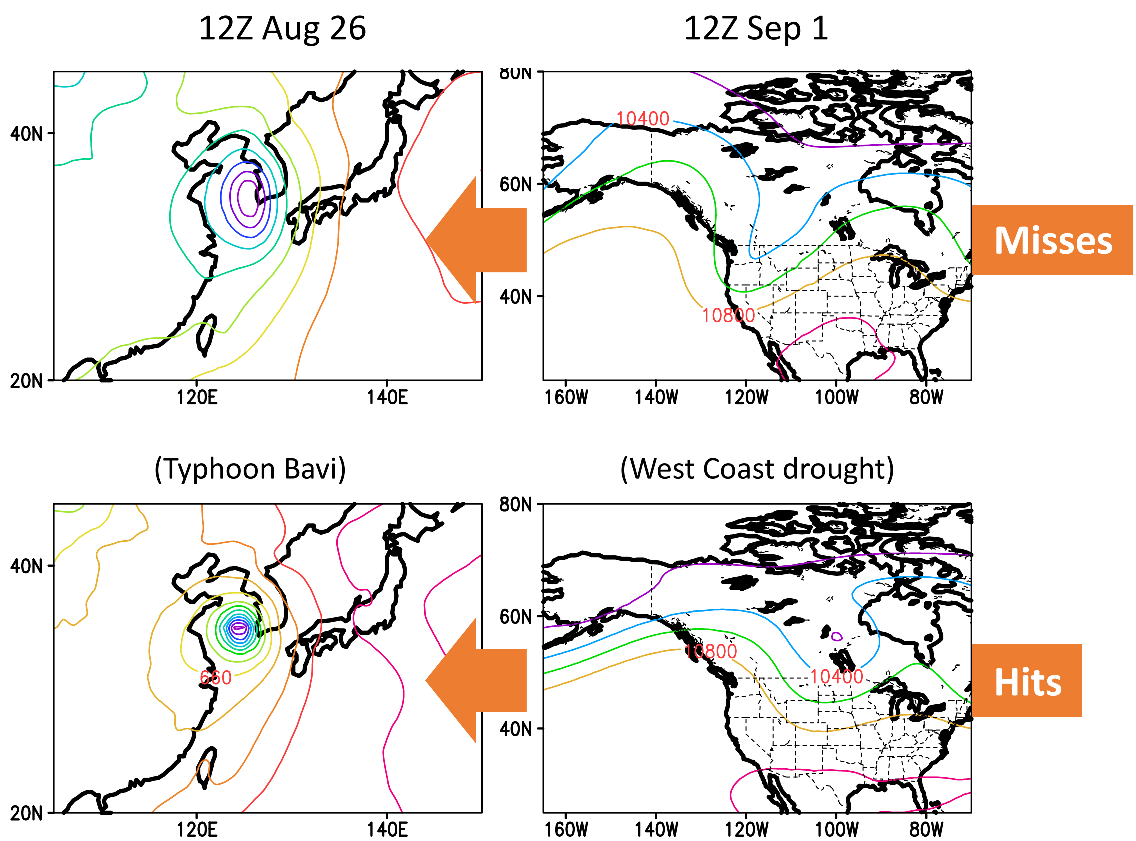

Figure S3. Same as Figure S1 but for September 1's ridge buildup in western North America and associated forecast difference of Typhoon Bavi.